JOURNAL OF GEOPHYSICAL RESEARCH, VOL. 110, B03302, doi:10.1029/2004JB003299, 2005

Surface ruptures and building damage of the 2003 Bam, Iran, earthquake mapped by satellite synthetic aperture radar interferometric correlation

E. J. Fielding,[1,2] M. Talebian,[3] P. A. Rosen,[1] H. Nazari,[3] J. A. Jackson,[2] M. Ghorashi,[3] and R. Walker[2]

Received 6 July 2004; revised 17 November 2004; accepted 15 December 2004; published 4 March 2005.

[1] We use the interferometric correlation from Envisat synthetic aperture radar (SAR) images to map the details of the surface ruptures related to the 26 December 2003 earthquake that devastated Bam, Iran. The main strike-slip fault rupture south of the city of Bam has a series of four segments with left steps shown by a narrow line of low correlation in the coseismic interferogram. This also has a clear expression in the field because of the net extension across the fault. Just south of the city limits, the surface strain becomes distributed over a width of about 500 m, probably because of a thicker layer of soft sedimentary material. Another fault north of Bam shows offset and low correlation over a wider zone in the interferograms, but it has no discrete surface rupture, possibly because of a net shortening across this fault. Taking the difference between the interferometric correlation for an interval including the earthquake and an interval before the earthquake separates the changes due to the earthquake from other effects in the partially vegetated city of Bam. We map the damage to buildings by measuring the change from high correlation to low correlation where buildings were destroyed by the earthquake.

Citation: Fielding, E. J., M. Talebian, P. A. Rosen, H. Nazari, J. A. Jackson, M. Ghorashi, and R. Walker (2005), Surface ruptures and building damage of the 2003 Bam, Iran, earthquake mapped by satellite synthetic aperture radar interferometric correlation, *J. Geophys. Res.*, *110*, B03302, doi:10.1029/2004JB003299.

1. Introduction

[2] On 26 December 2003 at 0527 LT, a moderately large earthquake (M_w = 6.6, seismic moment 6–8 × 10^{18} N m) struck the small city of Bam in the Kerman province of southeast Iran (Figure 1). The intense shaking in the city caused the complete collapse of nearly every building in the central parts of the city including many of the newer buildings, killing at least 25,000 people officially (with early estimates as high as 40,000) out of a population of about 100,000–140,000. Four large earthquakes (M > 6) since 1981 [*Berberian et al.*, 1984, 2001] have occurred on the nearby Gowk fault zone (see Figure 1). The Gowk fault zone, a predominantly right-lateral strike-slip zone that extends from 50 km west of Bam northward [*Walker and Jackson*, 2002], has also been associated with several large historical earthquakes [*Ambraseys and Melville*, 1982; *Berberian and Yeats*, 1999]. An aseismic slip event was mapped by synthetic aperture radar (SAR) interferometry in the Shahdad fold-and-thrust belt about 50 km north of Bam [*Fielding et al.*, 2004] (Figure 1). There have also been other large earthquakes in the area in the last 40 years [*Engdahl et al.*, 1998] (Figure 1), but the city of Bam has not been affected by an earthquake for at least several hundred years. The World Heritage Site citadel, Arg-e-Bam, was constructed largely in the 1700s out of mud bricks [*Matheson*, 1976] and was destroyed by this earthquake. The city of Bam was a major stop on the Silk Road at least as far back as the fourth century A.D., and there are no historical reports of major earthquake damage in Bam. Seismic body wave and preliminary Envisat radar interferometry analysis shows that the main moment release of the earthquake was right-lateral strike-slip motion on a nearly vertical fault oriented roughly north-south [*Talebian et al.*, 2004]. Nearly all of the fault slip was shallower than 10 km depth, and the slip decreased above 1–2 km depth [*Talebian et al.*, 2004]. A N-S blind reverse fault believed to have been active during the late Quaternary, the Bam Fault, passes some 4 km east of the main part of Bam city and just to the west of Baravat [*Berberian*, 1976]. This fault does not appear to have moved significantly at the surface trace, but a deeper portion may have slipped during the 2003 earthquake [*Talebian et al.*, 2004; G. J. Funning et al., Surface displacements and source parameters of the 2003 Bam (Iran) earthquake from Envisat ASAR imagery, submitted to

[1]Jet Propulsion Laboratory, California Institute of Technology, Pasadena, California, USA.
[2]Centre for the Observation and Modelling of Earthquakes and Tectonics, Department of Earth Sciences, University of Cambridge, UK.
[3]Geological Survey of Iran, Tehran, Iran.

0148-0227/05/2004JB003299$09.00

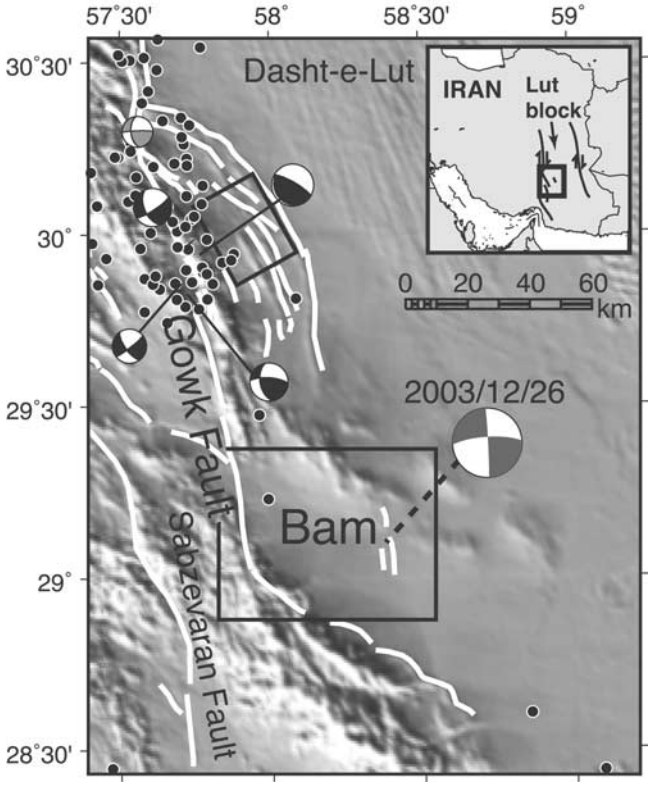

Figure 1. Region around Bam with shaded relief (GTOPO30) with light from azimuth 225°. Inset shows location and major strike-slip fault systems in eastern Iran. White lines are active faults, black circles are earthquake epicenters 1964–1998 from *Engdahl et al.* [1998]. Bam earthquake mechanism [*Talebian et al.*, 2004] is shown with medium gray quadrants. The Gowk fault is a major strike-slip fault on the western side of the Dasht-e-Lut (desert) block that has had four earthquakes $M > 6$ (focal mechanisms with black quadrants from body wave solutions of *Berberian et al.* [2001]) and one M_w 5.3 (gray quadrants from Harvard centroid moment tensor solution) since 1981. Aseismic slip event of 1998 beneath the Shahdad fold-and-thrust belt is shown as thin rectangle [*Fielding et al.*, 2004]. Note Bam earthquake mechanism is plotted at larger scale than previous earthquakes. Box shows extent of Figure 2.

Journal of Geophysical Research, 2004, hereinafter referred to as Funning et al., submitted manuscript, 2004]. The area where the city of Bam is located is underlain by young sedimentary rocks of unknown thickness, and only a few tens of meters are exposed in the small fold just west of the Bam Fault (Figure 2). Preliminary mapping of the surface ruptures and estimation of the fault dislocations at depth were presented by *Talebian et al.* [2004] on the basis of field observations as well as both the interferometric phase and correlation. Funning et al. (submitted manuscript, 2004) have performed an in-depth analysis of the locations of and slip distribution on faults at depth on the basis of the interferometric phase of these and other interferograms. Here we present a more detailed analysis of the surface changes associated with the Bam earthquake measured by satellite imagery (primarily radar) to map the location and types of surface ruptures and estimate the areas of major damage to buildings. In this paper we concentrate on the use of interferometric correlation measurements, which are a measure of the coherence of the synthetic aperture radar reflections from the surface.

2. SAR Data and Correlation Analysis

2.1. Interferometric Processing

[3] We formed interferograms from three pairs of European Space Agency Envisat synthetic aperture radar (SAR) images: on the descending (satellite moving south) track 120, one pair covering a half-year interval before the earthquake and the other for 35 days including the earthquake, and on the ascending track 385, one coseismic pair covering 70 days (see Table 1). The interferograms were processed from the Envisat advanced synthetic aperture radar (ASAR) level 0 (raw data) products using the ROI_pac (version 2.3) software [*Rosen et al.*, 2004] with 1 range and 5 azimuth looks (SAR "looks" are samples averaged [*Rosen et al.*, 2000; *Bürgmann et al.*, 2000]) to produce approximately 20 × 20 m cells (pixels) on the ground. The perpendicular component of the interferometric baseline is 570 m for the descending coseismic pair (i2) and 470 m for the preseismic pair (i1 in Table 1). Both descending pairs have baselines that are longer than commonly used for interferometry, so the topographic component of the interferometric phase was large and more difficult to remove. We used the newly released Shuttle Radar Topography Mission (SRTM) digital elevation model [*Farr and Kobrick*, 2000] with a 3-arc sec posting to calculate and remove the topographic component [*Rosen et al.*, 1996, 2004]. The ascending pair had a small baseline. The Envisat satellite on descending orbits looks to the right (west), and the imaging swath (or beam) 2 used here has an angle of 23° from the vertical at the center of the swath. The city of Bam is close to the center of the descending track 120 data that we analyze here (i1 and i2 in Table 1), but it is close to the edge of the ascending track 385 (i3 in Table 1). The look azimuth (relative to the Earth surface) varies with latitude and is approximately 77° west of north (azimuth 283) for the descending scenes and 77° east of north for the ascending scenes used here. Long-wavelength orbit errors were corrected by estimating an adjusted baseline to minimize the difference between the unwrapped phase and a simulated phase map [*Rosen et al.*, 1996, 2004]. Geocoding of results used easting and northing coordinates in UTM zone 40 and WGS84 datum. The ascending and descending coseismic pair unwrapped phases were combined to calculate two components of the surface motion. The sum of the two phases is largely up motion, with about 10% of north motion, and the difference between the two phases (descending minus ascending) is an approximation of the east motion. These simple components are not exact because the incidence angle varies across the swath, but the changes are gradual and have little effect on the short-wavelength features described in this paper.

2.2. Interferometric Coherence and Correlation

[4] Interferometric correlation measures how much the complex phase signal of the two SAR images is coherent at each location. If the distribution of radar-reflective objects

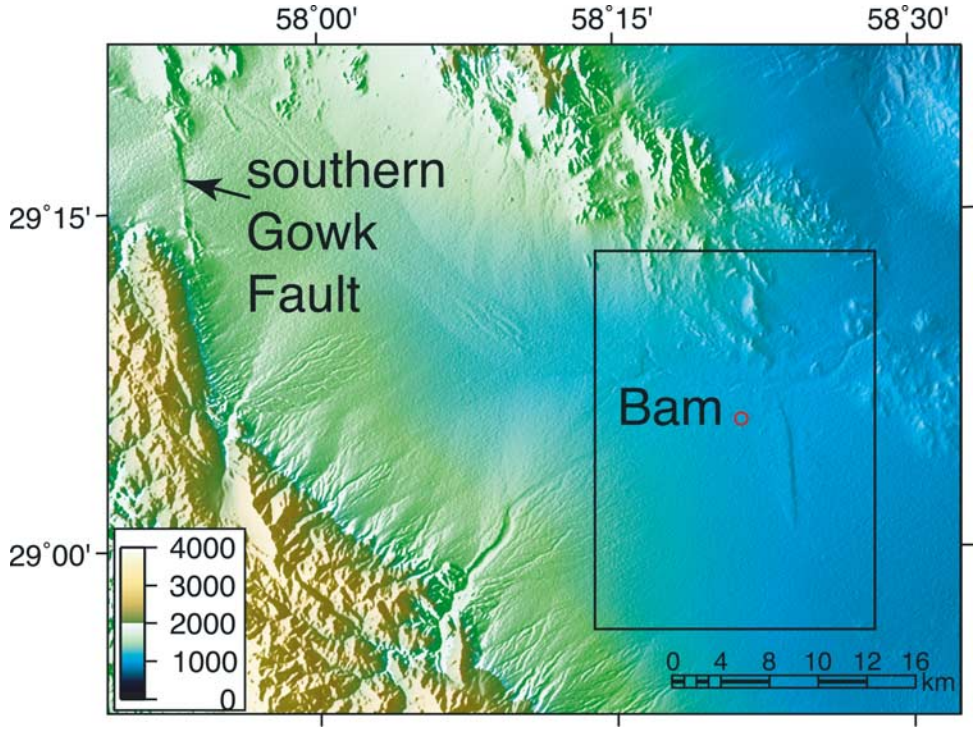

Figure 2. Topography of Bam area, from SRTM 3-arc sec data. Combination of shaded relief (illumination from azimuth 280°) with color proportional to height. The southern Gowk (Sarvestan) fault at the west side. The city of Bam is in a flat plain, but the small ridge of the Bam Fault between Bam and Baravat is visible in the shading. The small red circle shows the location of the Bam strong motion station, close to the center of the city. Box shows extent of Figure 3.

inside a SAR resolution cell (roughly 20 m in range, across-track, by 4 m in azimuth, along-track, on the ground for the Envisat data used here) changes during the time between the two image acquisitions, the interferometric coherence is reduced and a random modification (noise) added to the phase. The complex correlation function γ, defined as [e.g., *Hoen and Zebker*, 2000; *Rosen et al.*, 2000]:

$$\gamma = \frac{\langle g_1 g_2^* \rangle}{\sqrt{\langle |g_1|^2 \rangle \langle |g_2|^2 \rangle}} \quad (1)$$

is used to measure the interferometric correlation from the spatial statistics of the complex values g_i of the i = 1,2 images in the interferogram pair. The angular brackets denote averaging over an ensemble of radar observations, taken as adjacent SAR pixels. Correlation between the interferometric phase measurements in a small region (at least five SAR pixels) is used as an estimate of the signal coherence [*Zebker and Villasenor*, 1992; *Rosen et al.*, 2000]. For completely coherent radar scatterers, such as a corner reflector that does not change between the radar observations, the correlation $\gamma = 1$. If the radar scatterer is completely different for the two observations $\gamma = 0$. We will be using the magnitude of the complex correlation $|\gamma|$ here.

[5] An important aspect of the spatial averaging in (1) is that the correlation estimate can be biased downward by a phase gradient across the averaging window [*Bürgmann et al.*, 2000]. The known phase gradients due to the interferometric baseline and topography can be removed prior to calculating the correlation, but other phase gradients such as those due to coseismic deformation of the surface over a few hundred meters are more difficult to remove. Using a smaller averaging window reduces the effects of phase gradients, but it then causes a tendency to overestimate the correlation in areas of low correlation due to the small number of points [*Hoen and Zebker*, 2000; *Bürgmann et al.*, 2000]. *Hoen and Zebker* [2000] describe a way to correct for this bias, but we did not use that here as we are not interpreting the correlation values, only their spatial characteristics. These computation effects are independent of the physical causes of decreased correlation discussed in section 2.2.

[6] An alternative, but related, way to calculate the correlation is to use the phase variance σ_ϕ^2. The σ_ϕ^2 is computed in ROI_pac by deramping a region (removing a

Table 1. Envisat ASAR Interferograms Used for This Study

Type	ID	Date 1	Date 2	Direction	$B_\perp$ [a]
Preseismic	i1	11 June 2003	3 Dec. 2003	descending	468–470
Coseismic	i2	3 Dec. 2003	7 Jan. 2004	descending	577–583
Coseismic	i3	16 Nov. 2003	25 Jan. 2004	ascending	40–64

[a]Perpendicular baseline (meters) at center of swath.

local ramp or phase trend), then measuring at the variance of the phase in the region. We call phase-sigma correlation the correlation computed from the standard deviation, σ_ϕ. From the formula relating the phase variance or standard deviation to the correlation [*Rodriguez and Martin*, 1992; *Rosen et al.*, 2000]:

$$\sigma_\phi = \frac{1}{\sqrt{2N}} \sqrt{\frac{1-\gamma^2}{\gamma^2}} \quad (2)$$

where N is the number of samples, one can compute γ (or more precisely $|\gamma|$) from an estimate of σ_ϕ. Both methods of calculating the correlation were used in results presented here.

2.3. Interferometric Correlation Components

[7] Correlation is a measure of the coherence of the radar wave field, as well as other samenesses or differences in the data. Wave field coherence is an element of interferometric correlation, but there are also noise effects such as quantization noise, thermal noise, and processing noise that contribute to correlation decreases. Effects that decrease the correlation are often called "decorrelation" in the radar literature, but we use the term correlation decrease here to avoid confusion. In addition, baseline separation and volumetric and scattering effects cause loss of coherence of the wave fields and the addition of noise. The complex correlation function can be broken up into these correlation components [*Rosen et al.*, 2000; *Zebker and Villasenor*, 1992]:

$$\gamma = \gamma_N \gamma_G \gamma_V \gamma_T \quad (3)$$

where γ_N is correlation due to thermal noise in the SAR system, γ_G is geometric (baseline) correlation, γ_V is volumetric correlation, and γ_T is temporal (changes over time, including those caused by an earthquake) correlation. These components each contribute to lowering the overall interferometric correlation because they are multiplied, unlike the additive components of interferometric phase.

[8] The thermal noise of the radar hardware system and the SAR processing software introduces noise in the interferometric phase and decreases correlation [*Zebker and Villasenor*, 1992; *Rosen et al.*, 2000]. Included in this noise term are reductions in correlation due errors in processing parameters such as the registration between the two images of the interferogram. This noise component of the correlation γ_N can be treated as additive noise [*Rosen et al.*, 2000]. Because of the way that the correlation is calculated (1), this additive noise causes an upward bias in the correlation so that areas with zero wave field coherence have a correlation $|\gamma| > 0$, typically in the range of $0.2 < |\gamma| < 0.4$ with a white noise or "speckle" pattern.

[9] The geometric correlation component γ_G is due to the baseline (distance between orbits, measured perpendicular to the radar line of sight, $B_\perp$) of the interferogram. It has a complicated statistical expression that depends on the details of the radar response [e.g., *Rosen et al.*, 2000] that would be expected to decrease approximately linearly from 1 with a baseline of zero length to 0 at the critical baseline length of the SAR system [*Zebker and Villasenor*, 1992]. Because the two Envisat interferograms used here have very long baselines, on the order of half the critical baseline of 1100 m (Table 1), the geometric correlation decrease effect alone could reduce the correlation to 0.5 or less, even without including the other factors of equation (3). Fortunately, applying a bandpass filter to shift the center frequencies of the two SAR images can compensate for the geometric effect [*Gatelli et al.*, 1994]. The optimum spectral shift depends on the radar look direction and the slope of the ground surface. The ROI_pac software applies this shift assuming zero surface slope, which works well for Bam and the surrounding areas that have very shallow topographic slopes (Figure 2) and produces correlation values well over 0.9.

[10] The third contribution to correlation in (3), γ_V, is due to volumetric scattering or reflection of the radar waves from a volume of material, typically vegetation. This volumetric correlation decrease effect can be related to the density and height of vegetation and also depends on the baseline [*Zebker and Villasenor*, 1992; *Rosen et al.*, 2000]. The 56 mm (C band) wavelength of the Envisat radar means that the correlation is sensitive to objects that are about 10 mm across and larger. This means that it is substantially affected by the leaves, branches and trunks of trees and bushes. The desert areas around Bam are completely unvegetated, generally giving high correlation where there are no other changes, but there are extensive groves of date trees in the city of Bam and adjacent Baravat, resulting in lower correlation.

[11] The final component of correlation, γ_T, is the temporal correlation decrease that occurs when the radar scatterers in a SAR pixel change during the time interval of the pair. This component only affects repeat pass interferometry where the two images are taken at different times, unlike the other components that also affect single-pass interferometry. Areas with high correlation had almost no modification to the surface objects during that time interval, while other areas with low correlation had major modifications. This makes the interferometric correlation a sensitive measurement of earthquake damage to both natural surfaces (such as fault ruptures) and human structures. One important complication is that many plants have 10 mm and larger leaves and branches that move in the wind or even grow during the time interval between the two SAR images, causing temporal correlation decreases in addition to the volumetric correlation decreases in C band interferograms. The short time intervals of the Envisat pairs used here (Table 1), combined with low relief and a lack of vegetation, gives generally high coherence in the interferograms.

3. Observations of Correlation Decreases

[12] The interferometric correlation of the coseismic pair of scenes measures the changes in the surface during the 35 days including the earthquake (Table 1 and Figure 3). In practice, we look at where the correlation has decreased (or decorrelation signals) to see the surface changes. The correlation images of Figures 3a–3c were calculated using (1) from the basic 1 range look and 5 azimuth look ($\approx$20 $\times$ 20 m) interferograms after removing the baseline or "orbital" phase variation with an averaging window of 5 by 5 pixels and a triangular weighting function. This gives an effective number of pixels in the averaging of

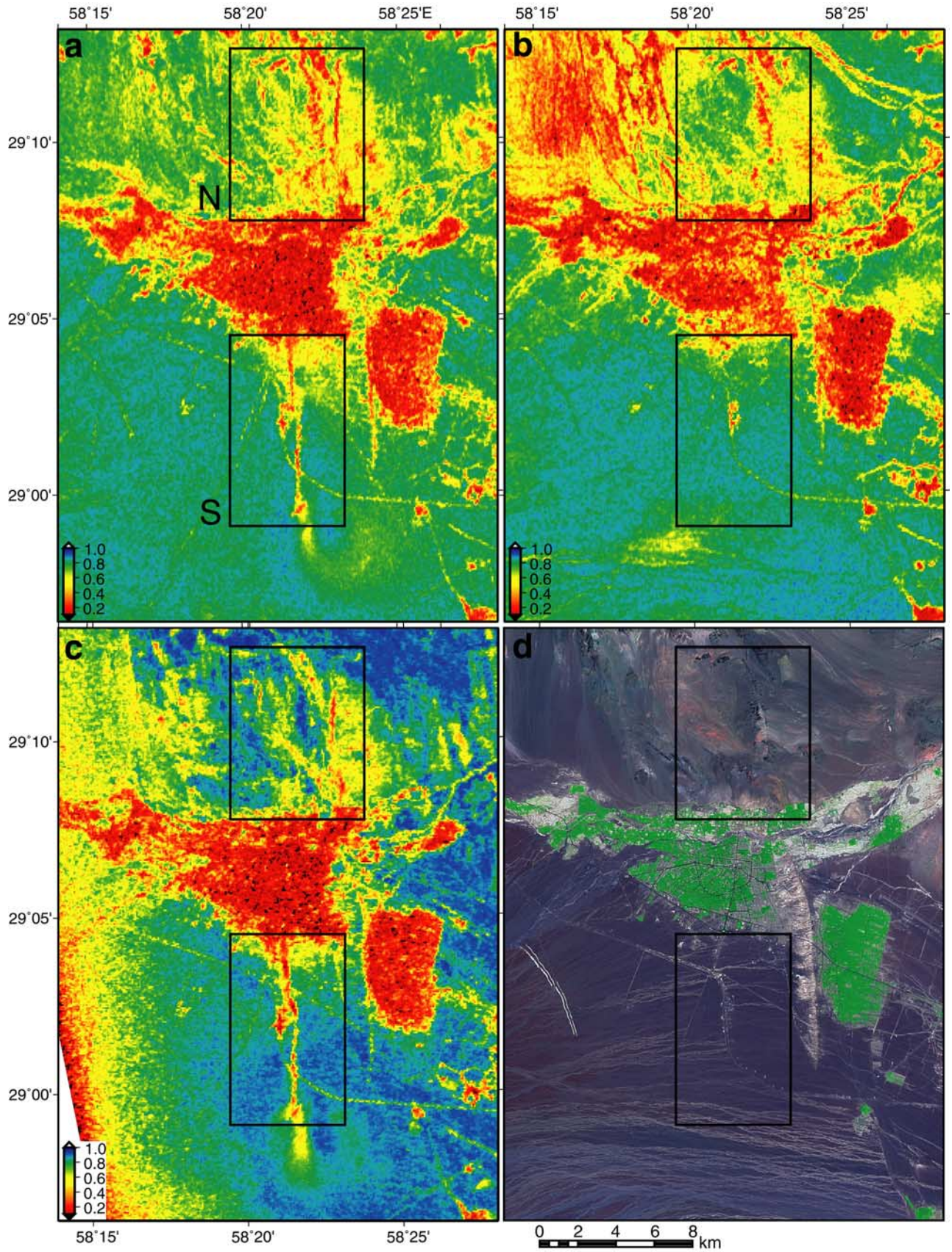
58°15'
58°20'
58°25'E
58°25'
a
b
c
d
N
S
29°10'
29°05'
29°00'
1.0
0.8
0.6
0.4
0.2
0 2 4 6 8 km

Figure 3

$2.5 \times 2.5 \times 5 \approx 31$ samples and a maximum spatial resolution of about 60 m, but further 4×4 averaging of the correlation data increases the pixel size to 80×80 m. Almost all the region surrounding Bam is completely barren desert (see Figure 4), so vegetation does not cause lower correlation there, but the irrigated tracts of Bam and Baravat (green in Figure 3d) have many trees, especially the date palms for which the Bam area is famous, that cause natural low correlation. Across the southwest corner of the correlation map from the ascending track, the correlation is strongly reduced by the lower signal-to-noise ratio at the edge of the SAR swath (due to lower γ_N in equation (3)). The swath width was extended with partial chirp processing that causes a gradual degradation of the signal at the edge of the swath (and therefore a reduction in correlation due to a higher noise level compared to the signal).

3.1. Correlation Decreases Due to Surface Ruptures

3.1.1. Ruptures South of Bam

[13] As described by *Talebian et al.* [2004], before the Envisat interferometric SAR (InSAR) was available, it was assumed that the previously mapped Bam Fault (a blind reverse fault, expressed as an asymmetric anticline at the surface) between Bam and Baravat was part of the fault system that ruptured in the 26 December 2003 earthquake. After we made the coseismic interferogram, we realized that the main surface rupture south of the city of Bam was about 4 km to the west of the Bam Fault because there was a line of strongly decreased correlation at that location and a high gradient in the interferogram phase [*Talebian et al.*, 2004]. The surface ruptures south of Bam were confirmed in the field on 31 January and 1 February 2004 [*Talebian et al.*, 2004], and further mapped on 29 March 2004 (Figure 4) at the location of the low-correlation signatures (Figures 3 and 5). These ruptures cut across an alluvial surface with a cemented gravel layer (approximately 5 cm thick) or desert pavement at the surface (Figure 4a). This alluvial fan or bajada surface slopes roughly eastward beneath the city of Bam and the area to the south (Figures 2 and 3).

[14] Figure 5a shows the correlation calculated with (1) from the full resolution interferogram (roughly 20×20 m spacing), with only the averaging of 5 pixels (5 looks) in the azimuth direction. Because there are only five samples averaged, the correlation estimate is very noisy. A little smoothing of the correlation (Figure 5b) shows some major features better, but necessarily reduces the resolution. The southern rupture is visible as four major segments (A–D) with steps to the left between them (Figures 3 and 5). Other low correlation south of Bam is associated with the train station (T on Figure 5), railroad, and roads (Figures 5a, 5b, and 5d). Field measurements of the northern three of these segments, A–C, showed right-lateral strike-slip horizontal offsets between 10 and 250 mm across the ruptures (Figure 4e). The southernmost rupture, segment D, had a continuous sharp rupture about 1 km long, trending N50–60°, with a right-lateral offset of about 5 cm and a vertical offset of about 12–13 cm downthrown to the southeast. The mapped field locations even match the smaller subsegments of segment B that are separated by smaller left steps (Figures 5a and 5b). The ruptures are not visible on the 15 m resolution Advanced Spaceborne Thermal Emission and Reflection Radiometer on the Terra satellite (ASTER) visible and near-infrared (VNIR) image acquired after the earthquake on 2 January 2004 (Figure 5d) as they did not cause major changes to the VNIR reflectance.

[15] All of the four segments of the southern rupture have an extremely narrow band of decreased correlation on the Envisat InSAR (Figures 5a and 5b). In the unfiltered correlation map, the low correlation is limited to a width of 2 pixels (40 m) at many points, with very high correlation next to this narrow zone. This indicates that the surface changes associated with the fault rupture were only close to the actual rupture. The adjacent desert pavement (see Figure 4a) was not significantly disrupted where the coseismic correlation is greater than about 0.8 (Figures 5a and 5b). This is especially true for the southern three segments, B–D. There were no strong motion instruments close to this southern rupture zone, but there was one located in the city of Bam, (see Figure 3). The area north of Bam had more widespread surface disruption (see Figure 6). We discuss this more in section 4.

[16] The visible surface rupture south of Bam ends at the north end of segment A (Figure 5b). Field investigation shows the area north of that has no significant surface rupture, only minor cracks with very small offsets. The InSAR phase measurements show a gradual ramp in the surface displacements here (Figures 5c and 7b), so the surface strain is spread over a distance of about 500 m. The full-resolution correlation is low over roughly the same 500 m wide zone where the surface strain is high (Figures 5a–5c) even though this correlation measure is insensitive to phase gradients. This would be consistent with distributed strain in the shallow subsurface, either inelastic or elastic deformation, above a fault at depth (see section 4). The east-west wall shown in Figure 4b (located at W on Figure 5b) was broken in four places over a similar distance, which also would be consistent with a wide zone of surface ruptures or with high accelerations. The asphalt road and wall at the south edge of the city of Bam showed some small cracks but no major ruptures, indicating that the surface here did not have concentrated strain.

[17] There is a wider area north of segment A and south of the city of Bam with somewhat reduced correlation (Figures 5a and 5b), despite a similar desert pavement surface. This may indicate a greater degree of shaking due to the earthquake in the area just south of the city than

Figure 3. Correlation and optical images of Bam area. All parts cover the same area, and boxes show locations of Figures 5 (S) and 6 (N). Correlation (Figures 3a–3c) calculated with a triangular weighting function over a 5×5 pixel window is shown in colors. (a) Correlation for descending track, coseismic interferogram (i2 in Table 1). (b) Correlation for interferogram before the earthquake (i1 in Table 1). (c) Correlation for coseismic interferogram on ascending track (i3 in Table 1). (d) Landsat 7 Enhanced Thematic Mapper image with bands 7, 4, and 2 as red, green, and blue and additional panchromatic band sharpening. Vegetation appears green in this false color image.

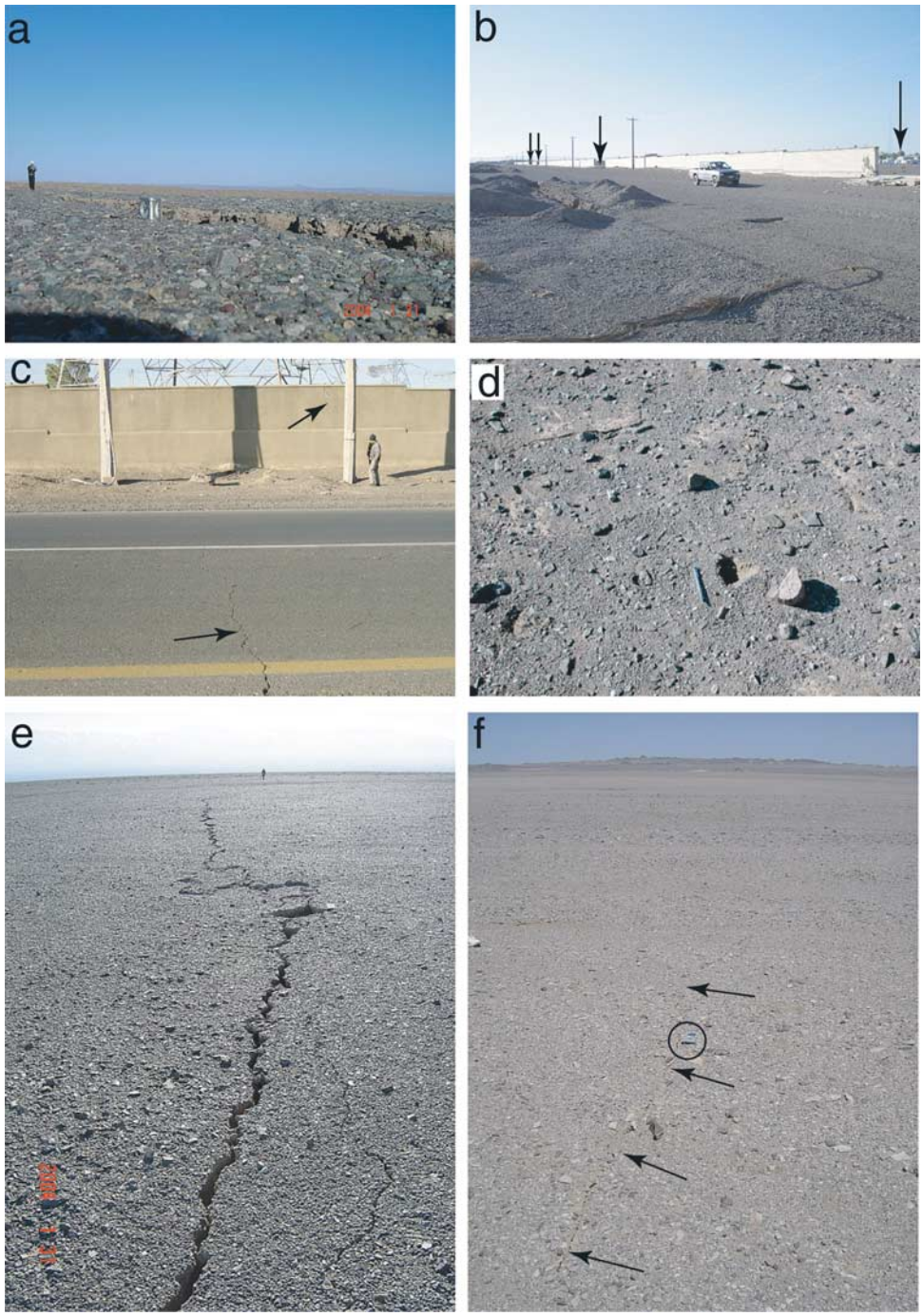

Figure 4. Field photographs of surface ruptures near Bam. (a) Rupture south of Bam in middle of segment C on Figure 5b, with vertical offset of about 5 cm in addition to horizontal offset. Desert pavement or cemented gravel surface in foreground. View is to northeast. (b) East-west wall and road at south margins of city of Bam, marked with W on Figure 5b. Arrows mark locations where wall was knocked down during the 2003 earthquake. View is to northwest. (c) Asphalt bypass road at southern edge of Bam with surface crack (marked with arrow), located about 500 m northeast of Figure 4b. Also note crack in wall to the left of person (also marked with arrow). View to north. (d) Stone dislodged from desert pavement and thrown about 10 cm, at location C in Figure 6b north of Bam. (e) Rupture in surface south of Bam at middle of segment C in Figure 5b. Right-lateral strike-slip offset of about 15 cm. View to south. (f) Minor crack in surface with trend NNE (marked with arrows) near south end of feature A in Figure 6b, view to NNE. Circle around compass for scale.

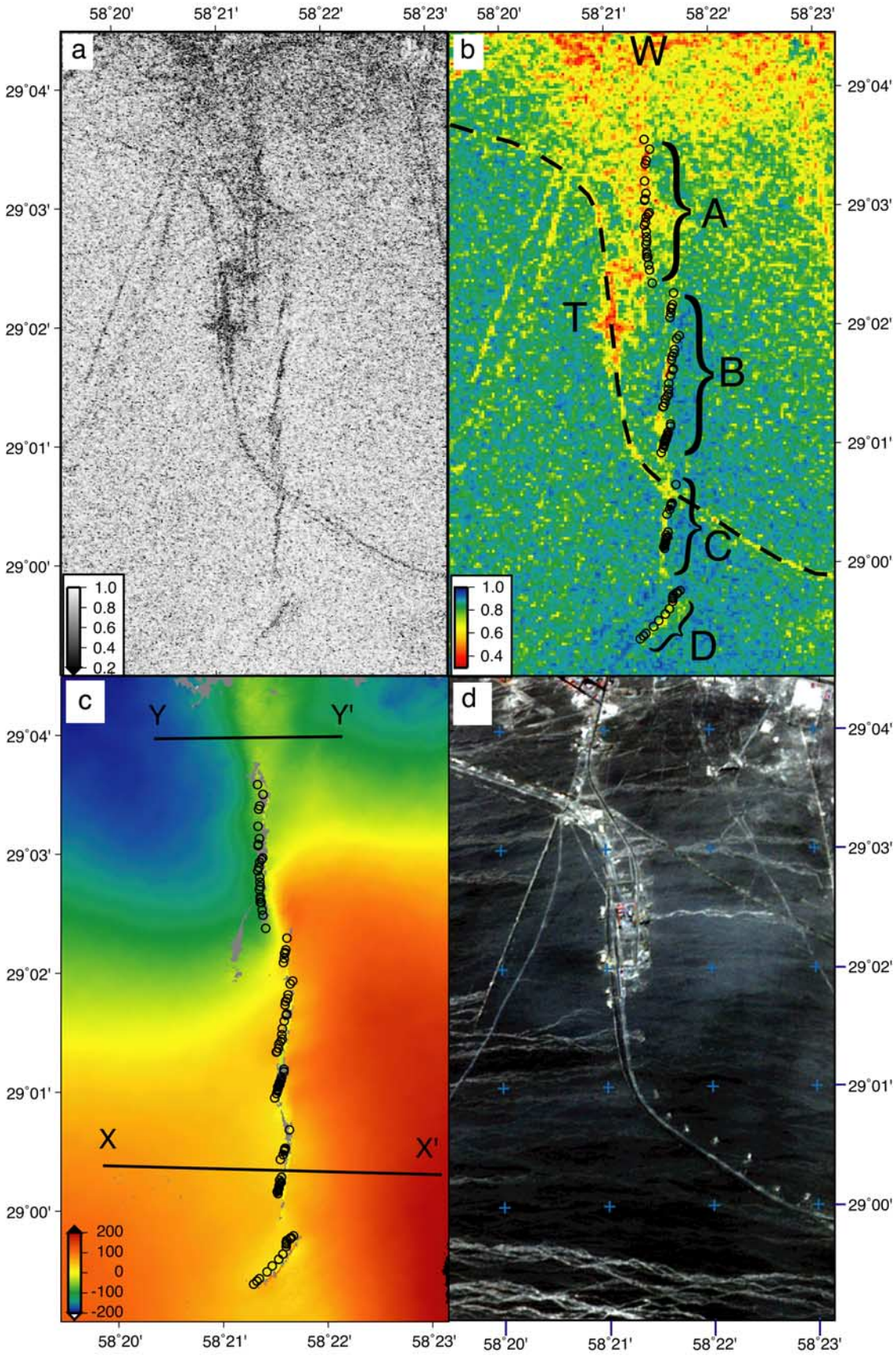
a
b
c
d
W
A
B
C
D
T
Y
Y'
X
X'
58°20'
58°21'
58°22'
58°23'
29°04'
29°03'
29°02'
29°01'
29°00'
1.0
0.8
0.6
0.4
0.2
200
100
0
-100
-200

Figure 5

adjacent to the other segments of the surface rupture south of Bam. Clearly, the city itself suffered severe damage from the earthquake. The damage to structures is discussed more in section 3.2.

3.1.2. Ruptures North of Bam

[18] The area to the north of the city of Bam is alluvial fans covered with desert pavement, similar to the area south of Bam, and there are several low-correlation features showing disruption of this surface. Unlike the ruptures south of Bam, there is decreased correlation on the coseismic interferogram over a wide area north of Bam and the background correlation is lower (Figure 3). Because of the generally lower correlation, we calculate the correlation here (see Figure 6a) with a greater amount of averaging to reduce noise, unlike the correlation shown in Figure 5. First the full-resolution interferogram was smoothed with a 3 × 3 pixel boxcar filter and then the correlation calculated with the phase-sigma method (equation (2)) with a rectangular, unweighted 5 × 5 pixel window, giving a resolution of about 120 m and roughly 200 total samples averaged.

[19] There is also some topographic relief on small hills north of Bam that causes low correlation due to the geometric or baseline correlation decrease effect (γ_G) with the long baseline of the coseismic, descending interferogram (i2 in Table 1), especially in the top center of Figure 6a. This geometric correlation is also present in the preseismic interferogram that also has a long baseline (i1 in Table 1; see Figure 3b). The spectral shift filter that we used does not compensate completely here for the long baselines of the descending interferograms due to the slopes on the hills. By precisely coregistering interferogram i1 with interferogram i2 and subtracting the two correlation maps (using the same phase-sigma correlation as in Figure 6a) we get a correlation difference map (see Figure 6b) that largely cancels out the geometric correlation effects. The correlation difference map shows areas with high correlation on the preseismic interferogram and low correlation on the coseismic interferogram in red, while blue areas have higher correlation in the coseismic interferogram than in the preseismic interferogram. The correlation difference map for the rest of the Bam area is described more below in section 3.2.

[20] In addition to the multiple patches of reduced correlation north of Bam (Figures 6a and 6b), there is one wide linear low correlation feature (marked A on Figure 6b). Field visits to the region north of Bam showed several minor ruptures, with one set of left-stepping cracks and small ridges (at B on Figure 6) almost continuous for about 2 km, with a small and difficult to measure right-lateral strike-slip offset [*Talebian et al.*, 2004]. At one location (marked C on Figure 6) near rupture B there was a rock dislodged from the cemented gravel layer and thrown about 10 cm (see Figure 4d). This type of thrown rock has been interpreted in other cases as indicating high acceleration at the surface (probably greater than 1 g or 9.8 m s^{-2}). This was the only rock observed to have been displaced, but the area was not studied in detail and the fairly widespread low correlation in this area indicates that there were other changes to the radar scatterers on the surface.

[21] The wide linear correlation decrease feature north of Bam (A on Figure 6b) was investigated in the field on 29 March. There was no sign of a significant surface rupture at this site, although there were some minor surface cracks (Figure 4e). There is a change in interferometric phase across this feature in both coseismic interferograms i2 and i3 (Table 1). By summing and differencing interferogram i3 (from the ascending track) and interferogram i2 (from the descending track) we can determine the east component (Figure 6c) and an "up" component that includes a small amount of the northward motion of the surface displacement, even though we can't determine the full three-dimensional displacement with only the phase of two interferograms [e.g., *Wright et al.*, 2004]. The east component of displacement is normal to the linear zone A and shows a net shortening of about 10 cm across the northern fault zone (Figures 6c and 7c), unlike the net extension across the southern rupture zone (Figure 7a).

[22] The feature marked D on Figure 6b was investigated in the field for signs of surface ruptures due to its prominent appearance of high albedo on ASTER imagery (Figure 6d) and a sharp topographic break (Figure 2). Only very minor cracking was found, along the base of a low hill. This hill is the cause of some geometric correlation decrease (γ_G) in both of the descending track interferograms (i1 and i2 in Table 1; see Figures 3a, 3b, 6a and 6b). The ascending track, coseismic interferogram (i3) has high correlation in this area (Figure 3c) because it has a much shorter baseline and therefore little geometric correlation decrease, indicating that the surface did not change significantly during the earthquake. The correlation difference map of Figure 6b, also shows that there is no significant change between the coseismic (descending track, i2) correlation compared to the preseismic (i1) correlation (differences are near zero). The geometric correlation decrease effect is similar for both interferograms as they have similar baseline lengths. This is consistent with the lack of significant surface ruptures here and confirms the absence of coseismic changes. Correlation differences are discussed more in section 3.2.

3.2. Correlation Difference Mapping of Building Damage

[23] In the city of Bam and the date plantation town of Baravat, there is a large decrease of correlation due to

Figure 5. Details of southern rupture zone, all panels cover same area. (a) Full-resolution correlation calculated from 1 × 5 SAR samples with 20 × 20 m spacing and no filtering on coseismic interferogram (i2 in Table 1). (b) Full-resolution correlation of Figure 5a after filtering with Gaussian filter (6σ width 120 m) with 40 m spacing (note different scale). Black open circles mark GPS locations of ruptures mapped in the field. Letters A–D indicate major segments of the surface rupture. Dashed line is railroad, and T is train station. W is location of wall in Figure 4b. (c) East component of surface displacement in mm, derived from difference of coseismic interferograms i2 and i3 (Table 1). (d) Postearthquake (1 February 2004) ASTER visible and near-infrared image with bands 3, 2, and 1 as red, green, and blue. Light colored smooth lines are railroad, roads, and power line tracks, most of which also have low correlation on Figures 5a and 5b. Irregular light lines are alluvial channels with occasional water flowing from the west.

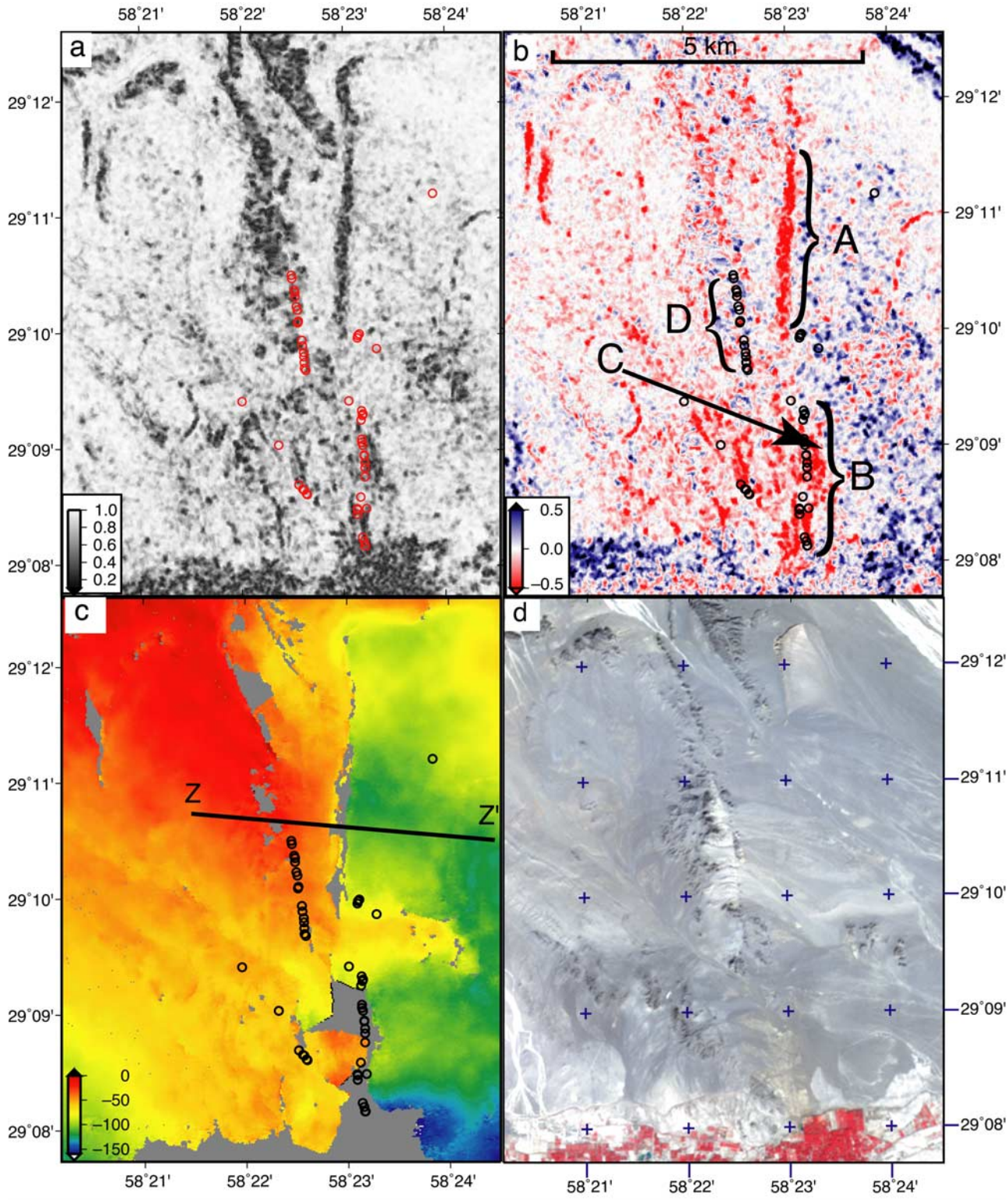

Figure 6. Details of ruptures in area north of Bam city. Panels cover same area. (a) Phase-sigma correlation calculated at roughly 100 m resolution. Red open circles mark GPS locations of ruptures mapped in the field. (b) Correlation difference between interferograms i2 and i1 (Table 1), using phase-sigma correlation. Red shows correlation decrease during coseismic interval. (c) East component of surface displacement in mm, derived from phase difference of coseismic interferograms i2 and i3. Note that displacement scale is smaller than in Figure 5c. (d) Postearthquake (1 February 2004) ASTER visible and near-infrared image with bands 3, 2, and 1 as red, green, and blue. Red areas at bottom of image are vegetation in fields on the north side of Bam.

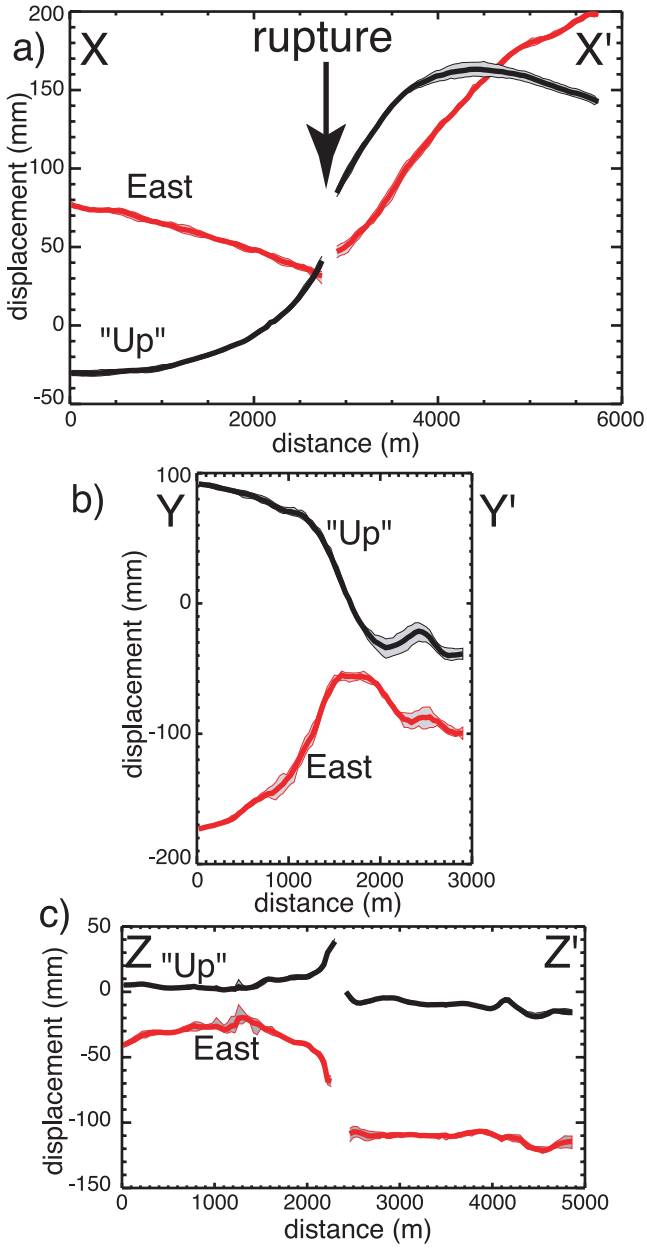

Figure 7. Swath profiles of surface displacement in mm projected in swath with width of 200 m. East and "up" components derived from combinations of coseismic interferograms i2 and i3 (Table 1). (a) profiles of surface displacement for south central part of rupture south of Bam along line X–X′ shown in Figure 5c. (b) profiles of northern part of rupture south of Bam along line Y–Y′ shown Figure 5c. (c) profiles of rupture north of Bam along line Z–Z′ shown in Figure 6c.

vegetation (green in Figure 3d), both from the γ_V and γ_T of equation (3). This low correlation is present in both the preseismic and coseismic interferograms (Figures 3a–3c). To separate the correlation decrease due to vegetation from correlation decrease caused by changes related to the earthquake, we took the correlation map for the 6-month pair (i1 in Table 1) before the event and subtracted it from the coseismic correlation map (i2 in Table 1) to produce a correlation difference map (Figure 8). Negative correlation change (red on Figure 8a) shows areas that were modified by the earthquake or other processes during the 35 days of the i2 interferogram interval, but were not modified in the previous 6 months. The damage to the city of Bam and surface fault rupture features (described in section 3.1.2) stand out on this correlation difference as strongly negative changes. Positive correlation differences (blue on Figure 8a) indicate areas that had surface changes in the 6 months from June to December 2003 but had little change during the coseismic interval. Zones with correlation differences near zero include areas with high correlation in both interferograms and areas with low correlation in both interferograms.

[24] When taking the difference of two images that have a substantial random noise component, including these correlation images, the signal-to-noise ratio is decreased. For the correlation difference maps, we used the phase-sigma correlation described in section 3.1.2, which has a spatial resolution of about 120 m and uses roughly 200 total samples. At locations where the correlation is low in both the coseismic and postseismic images, the "true" difference should be zero, but the random noise components do not cancel, resulting in a noisy difference estimate. Where the correlation is high in both images, the difference is very close to zero (such as the desert pavement surface south of Bam on Figure 8a).

[25] It should be noted that the preseismic (i1) and coseismic (i2) pairs (Table 1) used here for the correlation difference had similar baselines so the geometric and volumetric correlation effects were similar. If the baselines were very different, these effects might not cancel so completely. The correlation difference will work best when the baselines are similar.

[26] Most of the surfaces that changed in the preseismic interval, but not in the coseismic interval (giving a positive correlation difference or dark blue on Figure 8a) were affected by fluvial action (erosion or deposition). We confirmed this by calculating differences of optical images (ASTER) acquired before and after the earthquake (Figure 8b). The optical image differences can be calculated at the full resolution of the imagery (15 m for the ASTER VNIR bands) because of the low noise level. The mountains north of Bam must have had a large storm some time between June and December 2003 that caused extensive fluvial activity in the channels coming down toward Bam and in the main river through Bam. These channels have both positive correlation difference and positive visible image intensity change (dark blue at top left and top right on Figures 8a and 8b). The increase in the surface reflectance in visible wavelengths appears to be due to deposition of sand or erosion of dark material in the channels.

[27] The surface ruptures related the 2003 earthquake are not visible in the ASTER imagery, due to their small areal extent compared to the 15 × 15 m pixels. There are some negative changes in the surface reflectance at the optical wavelengths near the southern ruptures, but these are where there was construction activity on the railroad and railroad station, about 1 km to the west of the 2003 rupture. The large patch of negative change in the ASTER difference at the top of Figure 8b is due to a cloud shadow in the January 2004 image. The cloud itself is barely visible in the image

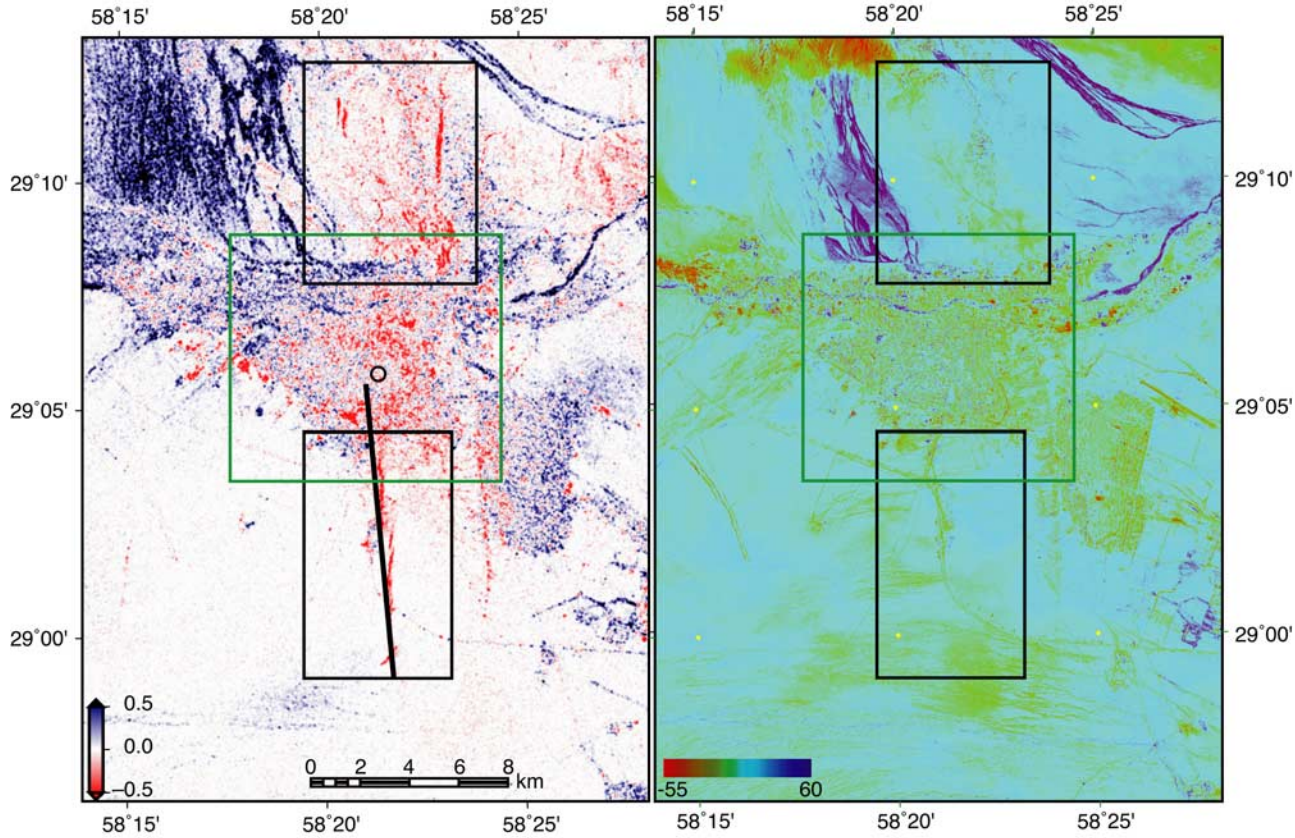

Figure 8. Difference images for the same area as Figure 3. Black boxes show locations of Figures 5 and 6, and green box shows location of Figure 9. (a) Correlation difference between coseismic correlation (i2) and preseismic correlation (i1 in Table 1). Positive correlation difference means correlation was higher during coseismic interval than during preseismic interval. Thick black line shows updip projection of main fault rupture determined from InSAR analysis (Funning et al., submitted manuscript, 2004). Black circle shows location of Bam strong motion station. (b) ASTER band 2 (red visible light) image (uncalibrated digital numbers) difference between image acquired on 2 January 2004 and image acquired on 8 March 2002. Positive difference means higher image intensity in 2004 image, with most increases due to fluvial deposits of bright sand on surface. Red and yellow areas (negative difference) at top due to cloud shadow in 2004 image.

and causes only a subtle effect on the difference image. The vegetated areas of Bam and Baravat have slightly negative differences that may be due to the difference in season of the ASTER images.

[28] The zones of strong decrease in correlation within the city of Bam (Figure 8), correspond closely to the damage mapped from airphotos taken just after the earthquake (27 December) by the *National Cartographic Center of Iran* (*NCC*) [2003] (Figure 9). The densely populated old parts of the city, where there was 100% destruction of the structures (marked as "total" destruction on Figure 9), had high correlation on the preseismic pair and low correlation on the coseismic pair giving correlation changes of −0.7 to −0.3. The NCC map, prepared for rescue operations, only outlines whole city blocks that were damaged and it includes some plots of date palms that are intermixed with the buildings so it cannot be used for a detailed comparison to the InSAR correlation map. The ancient city inside the outer walls of the Arg-e-Bam, where the mud brick buildings were completely flattened, also shows a very strong decrease in correlation (see area marked A on Figure 9). The large area of correlation decrease on the south edge of Bam (marked T on Figure 9) is a gravel covered plain next to the race track where aid workers installed a large city of tents to house the survivors whose homes were destroyed by the earthquake. This was verified on QuickBird imagery taken after the earthquake where the tents were starting to be installed.

[29] The use of single-pair InSAR correlation decreases for structure damage assessment was previously demonstrated for the Kobe, Japan earthquake [*Rosen et al.*, 2000], but the correlation difference map introduced here makes it possible to separate correlation decreases due to vegetation or other effects from earthquake damage. Areas of low correlation before the earthquake, such as those covered by trees or affected by baseline correlation decreases not changing with time, are subtracted from the coseismic correlation map to isolate the correlation decrease that happened in the coseismic interval. In this case, the first postearthquake Envisat image that could be used for SAR interferometry was acquired two weeks after the earthquake so some of the surface changes are caused by human

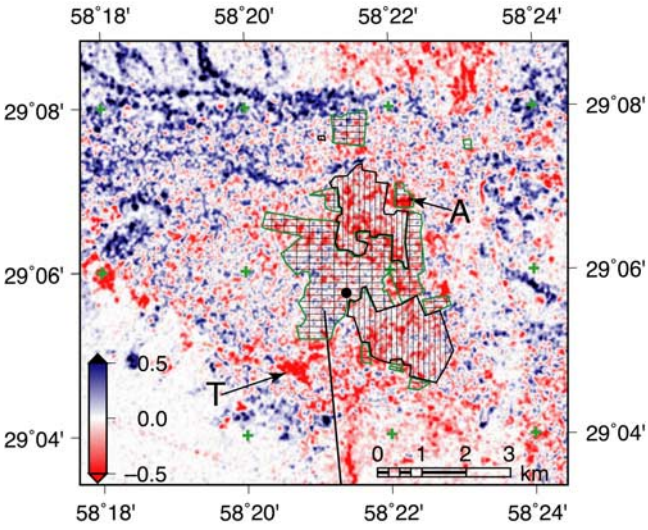

Figure 9. Correlation difference image detail for the city of Bam. Correlation difference between coseismic correlation (i2) and preseismic correlation (i1 in Table 1), enlarged from Figure 8. Positive correlation difference means correlation was higher during coseismic interval than during preseismic interval. Thick black line shows updip projection of main fault rupture determined from InSAR analysis (Funning et al., submitted manuscript, 2004). Solid black circle shows location of strong motion station. Areas with black outline and vertical line hatch were mapped as the "total damage" on the NCC preliminary damage assessment map [*National Cartographic Center of Iran*, 2003], and areas with green outline and both horizontal and vertical hatch were mapped as "very high" damage. The large low correlation patch marked with T is a formerly undeveloped desert area at the south edge of Bam where aid workers installed a large number of tents to house those made homeless by the earthquake. The very high damage polygon marked with A is the Arg-e-Bam castle complex that was heavily damaged by the earthquake.

activities in the rescue, temporary shelter, clean up and rebuilding phases.

4. Discussion and Conclusions

[30] Broad zones of decreased correlation (or decorrelation) have been previously observed around fault ruptures [*Simons et al.*, 2002]. The results presented here show that it is possible to map details of even minor surface ruptures by InSAR correlation with a high-resolution SAR system. In the Bam earthquake, the largest surface ruptures present an order of magnitude less offset than occurred at depth. We also show that it is possible to map changes in correlation due to the destruction of human structures. Because a number of radar samples are required to calculate the correlation estimate accurately and because earthquake damage can vary spatially, high-resolution SAR imagery is best for this kind of damage assessment. The multiple SAR beams on presently active satellites such as Envisat and Radarsat-1 can be used to revisit the site of an earthquake more quickly than the single-beam repeat interval of 35 days. To make interferometric measurements with different beams, a complete set of baseline (preevent) images should be acquired in all the high-resolution beam modes.

[31] The assessment of damage to buildings after an earthquake is most useful if it can be provided very quickly to rescue workers. Humans typically can only survive three days or less in a damaged building. Rapid damage assessment would require an InSAR system (either one satellite with a shorter repeat interval or a constellation of compatible satellites) that can revisit the site within a day or two after an event. New satellite systems with shorter repeat intervals are being built, including TerraSAR-X and the constellation COSMO-SkyMed. These systems have a shorter radar wavelength than the Envisat data used here (X band, roughly 3 cm) so they will have lower correlation in vegetated areas than the C band (5.6 cm) wavelength Envisat data used here, but should still have high correlation over buildings and other stable structures and surfaces. Additional issues for an operational disaster management system must also be addressed such as the need to get data quickly, process it in a timely way, and rapidly transfer usable products to the appropriate authorities.

[32] The ruptures south of Bam have clear expressions in both the correlation images and in the field. Some of the ruptures north of Bam show signs of minor surface cracks but no major ruptures. One significant difference between the ruptures south and north of Bam is that the southern rupture has a much larger offset at depth (perhaps as much as 3 m) [*Talebian et al.*, 2004] and a larger offset at the surface. The low-correlation feature marked A on Figure 6b is puzzling because it shows a strong coseismic decrease in correlation, but has no surface rupture visible in the field. The InSAR phase signal (Figure 7c) shows that there is a significant offset across this feature, but that it also includes a substantial shortening component. This may inhibit the opening of cracks in the cemented desert pavement, despite the shallow deformation revealed by the InSAR phase. The ruptures south of Bam have a large extension component (Figure 7a) that probably enhances the formation of surface cracks. This difference between the surface ruptures of faults with small differences in fault-normal offset could be important for relating field observations to active faults. Observed ruptures may be a biased sample of only faults with an extensional component in environments with desert pavements.

[33] Mapping surface ruptures with InSAR to guide field investigations is a powerful addition to the field seismologist's tool box [*Simons et al.*, 2002; *Talebian et al.*, 2004]. Understanding how surface ruptures relate to earthquakes by mapping present events is an important part of paleoseismology and risk assessment. In the case of the Bam earthquake, the surface ruptures were not found in the field until the InSAR correlation images were made [*Talebian et al.*, 2004]. The clear expression of the surface ruptures near Bam in the Envisat interferometric correlation images is largely due to the stable desert surface (see Figure 4). This completely unvegetated surface has no volumetric or temporal causes of correlation decreases at the C band wavelength of Envisat SAR, so the ruptures are clear. In other areas, where there is some amount of vegetation, a longer radar wavelength such as an L band (24 cm) system would be required to reduce the volumetric and other

temporal causes of low correlation and have a high enough preseismic correlation to detect the coseismic changes.

[34] The major fault slip that caused the 2003 earthquake occurred at depths below 1–2 km, beneath the surface ruptures south of Bam and extending northward beneath the center of the city [*Talebian et al.*, 2004; Funning et al., submitted manuscript, 2004]. As described above, the surface ruptures south of Bam stopped north of segment A in Figure 5, where the interferogram phase shows that the surface strain is distributed over a distance of about 500 m. This change in the mechanical behavior of the near-surface material may indicate that there is a thicker layer of unconsolidated or poorly consolidated sediments north of that point. Since there is a large river passing through the north side of the city of Bam, a thicker valley fill of river deposits extending beneath Bam and some distance to the south would not be surprising. The growing anticlinal structure east of Bam may have dammed the main river some time ago and caused thick deposits beneath the city that are now above the level of the river, in a way similar to the Safidabeh structure some 100 km east of Bam (B. E. Parsons et al., The 1999 Sefidabeh (eastern Iran) earthquakes revisited: New evidence from satellite radar interferometry and carbonate dating about the growth of an active fold above a blind thrust fault, submitted to *Geophysical Journal International*, 2004). This change in the near-surface materials is important for seismic risk evaluations because the presence of the active fault beneath the city would be difficult to detect beneath the thicker layer of softer material.

[35] The InSAR correlation also provides useful information on the effects of shaking on natural surfaces. This may allow at least qualitative evaluation of local ground shaking for earthquakes in areas where there are no strong motion sensors, potentially providing information on rupture mechanics or local amplification effects. The correlation in the area near the southern end of the main fault rupture south of Bam is greater than 0.9, significantly higher than any other area around the city, indicating that the surface here changed less during the earthquake. We speculate that the direction of the fault rupture caused less shaking in this area than elsewhere, despite its location near the surface rupture. This could be an example of the directivity effect if the fault rupture propagated from south to north [e.g., *Somerville et al.*, 1997], at least for the main part of the rupture. There was no strong motion sensor located near the southern end of the rupture, but there was one near the northern end (marked on Figures 2 and 8). At that location, which is about 400 m away from the surface projection of the fault rupture at depth [*Talebian et al.*, 2004], the strong motion instrument recorded a peak vertical ground acceleration of 1.0 g (9.8 m s^{-2}) (Building & Housing Research Center, Iran, http://www.bhrc.gov.ir/Bhrc/D-StGrMo/SHABAKEH/accelerograms/earthquake/2003/bam/bam.htm). This station showed that the city of Bam also suffered very high peak ground velocities of 0.4 m s^{-1} vertical and 1.4 m s^{-1} horizontal [*International Institute of Earthquake Engineering and Seismology*, 2004]. The area just south of the city of Bam also has widespread areas of moderately reduced coseismic correlation, even in the desert pavement area outside of the developed area. This suggests that the shaking here was more than the southern end of the rupture, causing more disruption of the surface, consistent with the strong motion record. It is extremely unfortunate that the vulnerable city of Bam was located at the northern end of the main earthquake rupture as this seems to be where the shaking was concentrated.

Notation

$B_\perp$ perpendicular component of baseline distance between antenna positions of interferometric pair
γ_N radar and processing noise component of correlation
γ_G geometric (baseline) component of correlation
γ_V volumetric scattering component of correlation
γ_T temporal change component of correlation

[36] **Acknowledgments.** We thank Barry Parsons for bringing up the subject of correlation in the Bam interferograms and Keith Priestley and Manuel Berberian for discussions. Eugenio Sansosti generously shared his program for reading Envisat level 0 data products. We thank Tom Heaton, Julian Bommer, and Yousef Bozorgnia for helpful advice on distance and directivity effects. We thank Gareth Funning for sharing results prior to publication. We thank Yuri Fialko and an anonymous reviewer for comments that helped to improve the writing. Part of the research described in this paper was carried out at the Jet Propulsion Laboratory, California Institute of Technology, under a contract with NASA. Research was also performed at the Centre for Observation and Modeling of Earthquakes and Tectonics (COMET), University of Cambridge, sponsored by the UK National Environment Research Council. We thank the European Space Agency for supplying the Envisat ASAR data under project AOE-668.

References

Ambraseys, N. N., and C. Melville (1982), *A History of Persian Earthquakes*, Cambridge Univ. Press, New York.

Berberian, M. (1976), Contribution to the seismotectonics of Iran, part II., Materials for the study of the seismotectonics of Iran, Rep. 39, Geol. Surv. of Iran, Tehran.

Berberian, M., and R. S. Yeats (1999), Patterns of historical earthquake rupture in the Iranian plateau, *Bull. Seismol. Soc. Am.*, *89*(1), 120–139.

Berberian, M., J. A. Jackson, M. Ghorashi, and M. H. Kadjar (1984), Field and teleseismic observations of the 1981 Golbaf-Sirch earthquakes in SE Iran, *Geophys. J. R. Astron. Soc.*, *77*(3), 809–838.

Berberian, M., J. A. Jackson, E. J. Fielding, B. E. Parsons, K. Priestley, M. Qorashi, M. Talebian, R. Walker, T. J. Wright, and C. Baker (2001), The 1998 March 14 Fandoqa earthquake (M_w 6.6) in Kerman province, southeast Iran: Re-rupture of the 1981 Sirch earthquake fault, triggering of slip on adjacent thrusts and the active tectonics of the Gowk fault zone, *Geophys. J. Int.*, *146*(2), 371–398.

Bürgmann, R., P. A. Rosen, and E. J. Fielding (2000), Synthetic aperture radar interferometry to measure Earth's surface topography and its deformation, *Annu. Rev. Earth. Planet. Sci.*, *28*, 169–209.

Engdahl, E., R. van der Hilst, and R. Buland (1998), Global teleseismic earthquake relocation with improved travel times and procedures for depth determination, *Bull. Seismol. Soc. Am.*, *88*, 722–743.

Farr, T., and M. Kobrick (2000), Shuttle Radar Topography Mission produces a wealth of data, *Eos Trans. AGU*, *81*, 583, 585.

Fielding, E. J., T. J. Wright, J. Muller, B. E. Parsons, and R. Walker (2004), Aseismic deformation of a fold-and-thrust belt imaged by synthetic aperture radar interferometry near Shahdad, southeast Iran, *Geology*, *32*(7), 577–580, doi:10.1130/G20452.1.

Gatelli, F., A. Monti Guarnieri, F. Parizzi, P. Pasquali, C. Prati, and F. Rocca (1994), The wave-number shift in SAR interferometry, *IEEE Trans. Geosci. Remote Sens.*, *32*(4), 855–865.

Hoen, E. W., and H. A. Zebker (2000), Penetration depths inferred from interferometric volume decorrelation observed over the Greenland ice sheet, *IEEE Trans. Geosci. Remote Sens.*, *38*(6), 2571–2583.

International Institute of Earthquake Engineering and Seismology (2004), Report on strong motion recordings for the Bam earthquake, technical report, Tehran.

Matheson, S. (1976), *Persia: An Archaeological Guide*, 2nd ed., Faber and Faber, London.

National Cartographic Center of Iran (2003), Preliminary damage map for Bam, Iran earthquake of 26 December 2003, Tehran.

Rodriguez, E., and J. M. Martin (1992), Theory and design of interferometric synthetic-aperture radars, *Proc. Inst Electr. Eng.*, *139*(2), 147–159.

Rosen, P. A., S. Hensley, H. A. Zebker, F. H. Webb, and E. J. Fielding (1996), Surface deformation and coherence measurements of Kilauea Volcano, Hawaii, from SIR-C radar interferometry, *J. Geophys. Res.*, *101*(E10), 23,109–23,125.

Rosen, P. A., S. Hensley, I. R. Joughin, F. K. Li, S. N. Madsen, E. Rodriguez, and R. M. Goldstein (2000), Synthetic aperture radar interferometry, *Proc. IEEE*, *88*(3), 333–382.

Rosen, P. A., S. Hensley, G. Peltzer, and M. Simons (2004), Updated Repeat Orbit Interferometry package released, *Eos Trans. AGU*, *85*(5), 35.

Simons, M., Y. Fialko, and L. Rivera (2002), Coseismic deformation from the 1999 M_w 7.1 Hector Mine, California, earthquake as inferred from InSAR and GPS observations, *Bull. Seismol. Soc. Am.*, *92*(4), 1390–1402.

Somerville, P. G., N. F. Smith, R. W. Graves, and N. A. Abrahamson (1997), Modification of empirical strong ground motion attenuation relations to include the amplitude and duration effects of rupture directivity, *Seismol. Res. Lett.*, *68*(1), 199–222.

Talebian, M., et al. (2004), The 2003 Bam (Iran) earthquake: Rupture of a blind strike-slip fault, *Geophys. Res. Lett.*, *31*, L11611, doi:10.1029/2004GL020058.

Walker, R., and J. A. Jackson (2002), Offset and evolution of the Gowk fault, S.E. Iran: A major intra-continental strike-slip system, *J. Struct. Geol.*, *24*, 1677–1698.

Wright, T. J., B. E. Parsons, and Z. Lu (2004), Toward mapping surface deformation in three dimensions using InSAR, *Geophys. Res. Lett.*, *31*, L01607, doi:10.1029/2003GL018827.

Zebker, H. A., and J. Villasenor (1992), Decorrelation in interferometric radar echoes, *IEEE Trans. Geosci. Remote Sens.*, *30*(5), 950–959.

E. J. Fielding and P. A. Rosen, Jet Propulsion Laboratory, California Institute of Technology, MS 300-233, 4800 Oak Grove Drive, Pasadena, CA 91109, USA. (eric.fielding@jpl.nasa.gov; paul.rosen@jpl.nasa.gov)

M. Ghorashi, H. Nazari, and M. Talebian, Geological Survey of Iran, P.O. Box 13185-1494, Tehran, Iran.

J. A. Jackson and R. Walker, COMET, Bullard Laboratories, Madingley Road, Cambridge CB2 0EZ, UK.